PHYSICAL REVIEW B VOLUME 60, NUMBER 24 15 DECEMBER 1999-II

Synthesis of epitaxial Fe_3O_4 films on Cu(001)

Richard L. Kurtz, J. Karunamuni, and R. L. Stockbauer
Department of Physics and Astronomy, Louisiana State University, Baton Rouge, Louisiana 70803
(Received 23 June 1999; revised manuscript received 25 October 1999)

Fe films, oxidized on a Cu(001) substrate, have been found to form large, uniformly thick patches of oxide that dominate the mesoscopic surface structure producing large, atomically flat terraces. The oxide is found to grow in highly oriented chains, many microns in length, with well-defined preferred orientations relative to the substrate crystalline axes. Under the oxidation conditions used here, Fe_3O_4 is the dominant oxide formed in thick films, a material with potential as a spin-polarized contact for magnetic tunneling devices.
[S0163-1829(99)51948-6]

Many materials have been investigated in multilayer heterostructures designed for magnetic sensors. Recently, it has been proposed that spin dependent transport could give rise to even more interesting devices and revolutionize the design of computational instrumentation.[1] Half-metallic materials, or materials with one spin orientation at the Fermi level, could play a significant role in bringing these new concepts to fruition.

Two classes of materials that have been proposed to be half metallic include the ternary Heusler alloys, such as $Ni_{1-x}Mn_xSb$, and a class of transition-metal oxides which include CrO_2. Andreev reflection measurements have recently shown that CrO_2 is indeed 90% spin polarized at the Fermi surface and other oxides such as $La_{0.7}Sr_{0.3}MnO_3$ display a significant spin polarization as well.[2] The application of these materials in realistic devices, however, is impeded by the need to produce the half-metallic material with high conductivity in a thin-film form. The control of stoichiometry in Heusler alloys tends to be problematic in thin films, and oxides are known to be notorious for their tendency to change oxidation state, driven by reactions at interfaces. One method to control the formation of undesirable oxidation phases is to use an oxide substrate whose lattice parameter matches that of the desired film. For example, CrO_2 is lattice matched with RuO_2 and TiO_2, but these substrates are not materials that are currently incorporated in devices.

Recent computation and measurements have suggested that other oxides may also display a significant spin polarization at the Fermi level. Fe_3O_4 is one such material, where computations suggest that the material is completely minority spin polarized at the Fermi level.[3] Early spin-resolved secondary-electron measurements observed a 40% spin polarization in the empty states near E_F.[4] It also has a relatively high electrical conductivity ($10^2\,\Omega^{-1}\,cm^{-1}$ at 300 K), unlike CrO_2, suggesting that it may perform better in device applications. In addition, its Curie temperature is 858 K, well above room temperature.

This material has been grown successfully on oxide substrates such as MgO and NiO, on the dissimilar metal Pt(111) and by decomposing the surface of single-crystal α-$Fe_2O_3(0001)$.[5–8] Various methods have produced high-quality Fe_3O_4 films, the preparation procedures striking a balance in growth parameters to avoid the formation of the undesirable iron oxide phases. Iron forms three common oxides, $Fe_{1-x}O$ (wustite), α-Fe_2O_3 (hematite), and Fe_3O_4 (magnetite). The heats of formation of these oxides are -272, -826, and -1121 kJ/mol, respectively, with the most stable phase being magnetite.[9]

On Pt(111), the $Fe_{1-x}O$ was found to form one monolayer thick on oxidation of submonolayer Fe. $Fe_3O_4(111)$ could be subsequently prepared by further Fe deposition and oxidation cycles, annealing in 10^{-6} mbar O_2 at 1020 K.[8] In the case of NiO and MgO, O-plasma assisted oxidation of evaporated-Fe films was found to produce Fe_3O_4 films for substrate temperatures between 540 and 570 K.[5,10] On Fe(110) at low O exposures, FeO initially forms, but in the presence of excess O_2 and in the temperature range of 300–500 K, a mixed oxide forms with Fe_3O_4 covered with α-Fe_2O_3.[11] Above 600 K, the α-Fe_2O_3 phase decomposes and Fe_3O_4 forms.

We report the growth of epitaxial $Fe_3O_4(111)$ films on Cu(001). Cu is commonly used in current device fabrication and we have found that it can be used as a malleable template for stable oxide growth. The oxide films develop a preferred orientation, forcing the substrate morphology to change, forming huge atomically flat terraces on the Cu substrate, an effect that can be extremely desirable in device growth. Since the cohesive energy of the oxide lattice is so large (11.6 eV per formula unit for spinel) it easily drives Cu steps to flow to provide the large terraces that are stabilized by the ionic lattice's Madelung energy.

We find two oxide phases form under our annealing conditions. For initial iron coverages below 2 monolayers, a single bilayer of $Fe_{1-x}O$ forms, and for thicker iron films the Fe_3O_4 spinel phase nucleates. These oxide layers are extremely stable and scanning tunneling microscopy (STM) results can be repeated successfully even after several days in vacuum. The epitaxy is also remarkable: the $Fe_{1-x}O(111)$ primitive cell has a $3.1\% \times 2.1\%$ compressive mismatch while the $Fe_3O_4(111)$ has an $0.7\% \times 0.32\%$ tensile mismatch with the Cu substrate in the [110] azimuths. This leads to the atomically flat oxide crystallites with micron dimensions.

Our oxide films were produced by oxidizing submonolayer to multilayer (<15 ML) Fe/Cu(001) for 5 min in 10^{-6} Torr O_2 at 835 K, and cooling in O_2 until 600 K. Oxidation of Cu is not observed to occur in our STM data and the (001) surface state was evident in photoemission for ox-

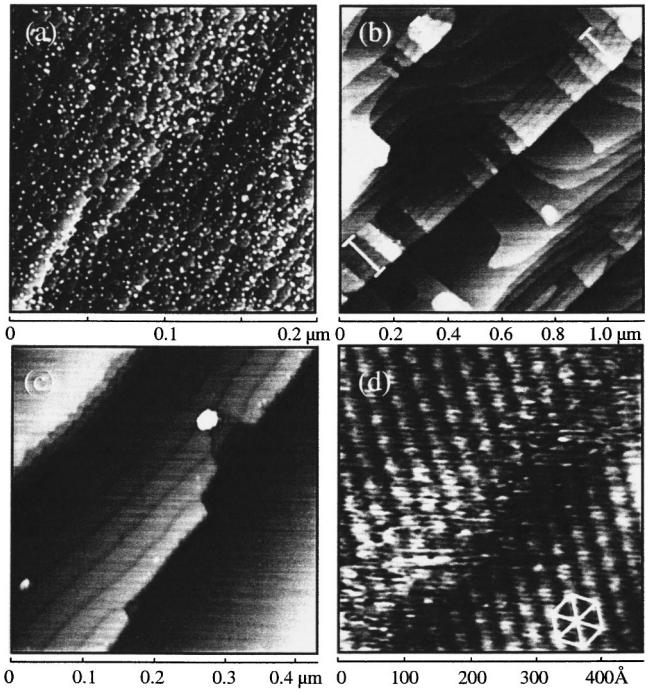

FIG. 1. (a) STM image of Cu(001) with 0.12 monolayers of Fe. Note the uniform atomically high step distribution of the substrate and small monolayer islands of Fe film. (b) Iron oxide formed after annealing. A long strip of oxide approximately 1800-Å wide and over 2-μm long is indicated, as well as others, with the white bars. The large flat terraces of Cu are bare of oxide and separated by single atomic-high Cu steps. (c) A close-up view of a 5-Å-thick strip of oxide showing dark stripes of antiphase domain boundaries and the four-layer internal structure near a defect. (d) Superlattice structure seen near a dark stripe.

ide films that did not completely cover the surface.[12]

Figure 1(a) shows submonolayer Fe deposited at room temperature. As observed previously, the Fe grows as tetragonally distorted fcc in a nearly perfect layer-by-layer mode on Cu(001) at room temperature, it undergoes the martensitic transition at ~10 ML to bcc Fe.[13] The (1×1) LEED patterns are slightly degraded from those of the clean Cu substrate.[13] When the Fe overlayer is annealed to 835 K in 10^{-6} Torr O_2, patches of oxide form, shown in Fig. 1(b). The growth of the first oxide phase is characterized by long strips along the Cu[110] and $[1\bar{1}0]$ azimuths with each strip oriented 90° from one another. The horizontal direction is the [100] of the Cu substrate in all of the images. Remarkably, the Cu substrate morphology changes to produce large flat terraces in the region of the oxide. When the oxide layer intercepts an atomically high Cu step, it forces the substrate to orient the step perpendicular to the {110} directions. We have observed that regions of the substrate free of oxide become more highly stepped, preserving the overall surface orientation.

The strips of oxide are found to include dark stripes that are separated by approximately 360 Å. These darker regions correspond to antiphase domain boundaries where strain relief causes a region with different atomic order and differing tunneling probability.[14] In Fig. 1(c), the internal layered structure of the oxide is shown at a defect with four distinct terminations amounting to a total of 5.0 Å in height, equivalent to two 2.48-Å-high bilayers in the $Fe_{1-x}O$ lattice.

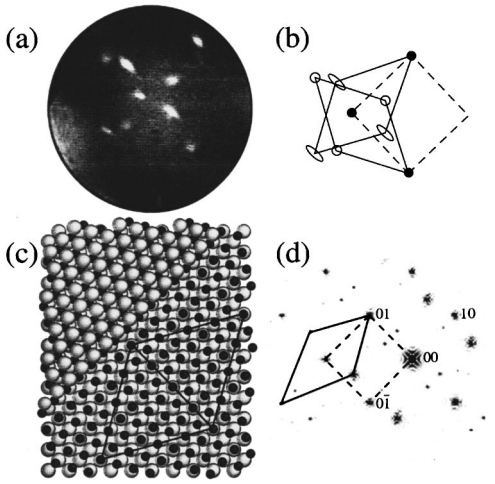

FIG. 2. (a) LEED pattern obtained at 60 eV from 2-ML Fe oxidized on Cu(001). The image consists of patterns from the two orientations, superimposed; one orientation shows streaked spots. (b) A schematic of the LEED pattern showing Cu substrate spots as filled dots, and the pattern from the two oxide domains as open circles and ellipses. (c) A model for $Fe_{1-x}O(111)$ on Cu(001). Fe^{2+} cations are the small dark circles and a step up to an oxygen layer is in the top left. (d) The Fourier transform of one domain of the structural model in (c), reproducing the domain orientation observed as streaked.

On closer inspection, the oxide has a hexagonal superstructure with an ~0.2 Å corrugation, as shown in Fig. 1(d). Although the oxide is conducting enough to allow the STM measurements, we were not able to obtain atomically resolved images. The separation of the hexagonal features is ~21 Å. The image in Fig. 1(d) shows this hexagonal periodicity near the region of one of the dark stripes. The rows of hexagons are mismatched on either side of the dark stripe by less than a single 21-Å cell, consistent with antiphase domain boundaries providing strain relief in these locations.

In Fig. 2(a), the low energy electron diffraction (LEED) pattern obtained from an oxidized 2-ML Fe film is shown. This pattern exhibits spots from the substrate as well as from the two orientations of oxide. In this particular film, one orientation formed preferentially, leaving disorder and/or small patches of the second oxide orientation. The disorder in the second orientation gives rise to the streaked LEED pattern for that domain, an effect which allows us to clearly separate the patterns from the two domains. This is illustrated schematically in Fig. 2(b) where one domain is given by open circles and the other with ovals. Regions of the surface have been observed in which neither domain exhibited significant streaking. This LEED pattern is only consistent with $Fe_{1-x}O$; both α-Fe_2O_3 and Fe_3O_4 would give additional spots not observed in Fig. 2(a). In Fig. 2(c), a model is provided for the orientation of the $Fe_{1-x}O$ oxide on the surface where the unit cell of the initial Fe layer is indicated relative to the Cu substrate. There are only two distinct ways in which this oxide can orient on Cu(001), and this gives the two 90° domains. The dimension of superlattice cell outlined in Fig. 2(c) is 21.06 Å. Presumably, a slight vertical rumpling of oxide within the superlattice gives rise to the pseudohexagonal structure in Fig. 1(d). In Fig. 2(d), a simu-

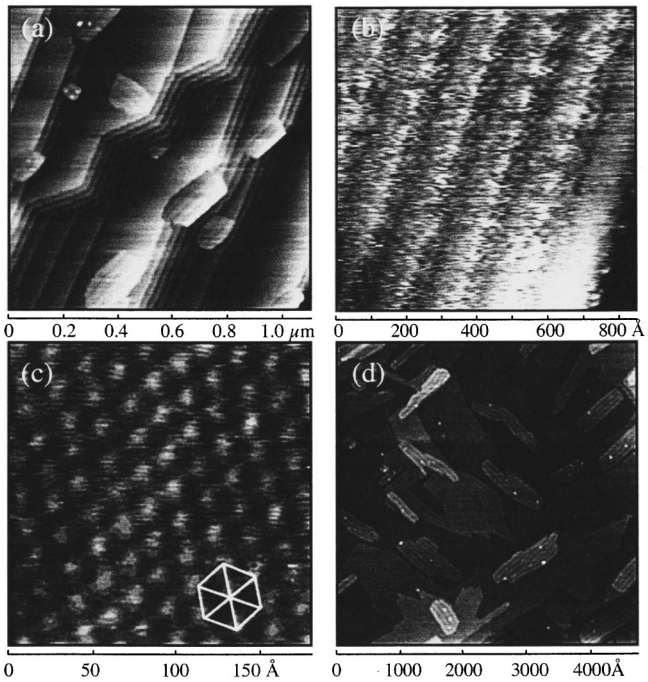

FIG. 3. (a) $Fe_3O_4(111)$ on Cu(001); note the hexagonal terminations of oxide steps; a few domains of FeO decorate the terraces. (b) A close-up view of a strip of oxide showing stripes with a 170-Å periodicity. (c) A closer view shows hexagonally arranged features separated by ~20.5 Å. (d) Thicker Fe films produce well-oriented oxide that completely covers the surface, sometimes exhibiting overlying patches of $Fe_{1-x}O$.

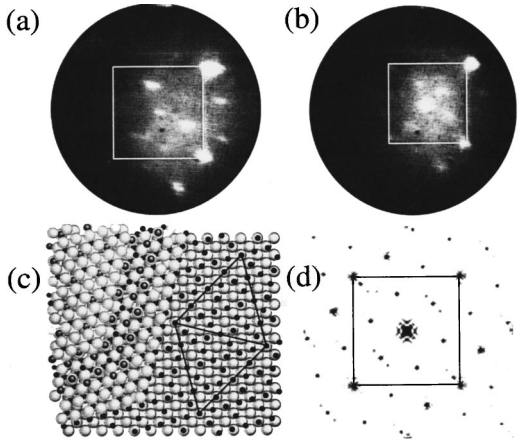

FIG. 4. LEED patterns obtained from Fig. 3(d) for (a) $E_p = 90$ eV and (b) $E_p = 125$ eV. (c) A structural model providing the domain orientation of the oxide observed in Fig. 3(a) and giving the origin of the 20.5-Å superlattice structure. In the model, the tetrahedral Fe are the small dark spheres, octahedrally coordinated Fe are larger, and oxygen ligands are given in successive layers to the top, left of the diagram. In (d), a simulated LEED pattern from a large-scale model of (c) is given, consistent with the observed data.

lated LEED pattern from the structural model in Fig. 2(c) shows that this orientation and lattice is consistent with the observed data.

With increasing Fe coverage, oxide films are found to grow in a second distinct phase, as shown in Fig. 3(a). These films have step edges oriented 15° from the [010] direction with well-ordered hexagonal step terminations consistent with a (111) orientation of the Fe_3O_4 oxide. Each terrace steps down to the other with a ~1.6-Å step height, although other heights such as 0.5 Å and 2.2 Å have been observed. The strain relief antiphase-domain structure on this oxide, Fig. 3(b), gives stripe structures separated by 170 Å and, due to the tensile strain, their morphology is distinct from those on $Fe_{1-x}O$. Close inspection also reveals a hexagonal superstructure with a similar 20.5-Å spacing, yet the orientation of the hexagon relative to the stripe is rotated 30° from that in $Fe_{1-x}O$, Fig. 1(c). For thick iron films, a complete surface oxidation can be found, as shown in Fig. 3(d). This oxide shows mostly the 170-Å-striped Fe_3O_4, but a few islands of the $Fe_{1-x}O$ can be found on top, in somewhat more random orientations.

In Figs. 4(a) and 4(b), we present the LEED patterns from this thick film for primary *e*-beam energies of 90 and 125 eV. The two energies provide different diffraction conditions that can be compared with simulated LEED data in Fig. 4(d). The Cu substrate spots are highlighted with the square overlay and the (00) beam is in the center. In Fig. 4(c), a model for the structure of $Fe_3O_4(111)$ on Cu(001) is given. $Fe_3O_4(111)$ consists of two metal layers separated by intervening oxygen. One Fe layer contains purely octahedrally coordinated Fe^{3+}, while the second Fe layer is actually a trilayer of Fe^{2+} and Fe^{3+} in mixed tetrahedral and octahedral sites. In the model of Fig. 3(b), we have drawn the interface terminated with the tetrahedral layer. To the top and left, we have shown successively thicker layers of Fe and O atoms in the spinel structure with an orientation appropriate to the domain diagrammed.

As seen in this model, the octahedrally coordinated (111) layer will align with the substrate if one considers a hexagonal unit cell which in the bulk spinel would be 20.57 Å. If the edge of this cell aligns with the Cu[110] direction, as shown, the lattice mismatch along that direction would be 0.7%. Perpendicular to this direction, the lattice mismatch is 0.32%. This model also results in two domains, as observed, which arises from the fact that the only other inequivalent orientation would be to align the cell boundary along the $[1\bar{1}0]$.

In order to confirm the structural model, we can take a two-dimensional (2D) Fourier transform of a large-scale model of Fig. 4(c) and this results in the simulated LEED pattern of Fig. 4(d). The orientation of the observed overlayer spots and their positions relative to those of the substrate are well reproduced.

Although the STM and the LEED data provide detailed information on the film and interface crystalline structures, they do not confirm specific oxidation states for the Fe at the interface or in the films. In ultrathin films with oxides less than or about a unit cell thick, one expects that the oxidation states will not be identical to those in bulk crystals with the proximity of the metal substrate perturbing the local electronic structure. In fact, our preliminary photoemission data show that the density of states at the Fermi level is much larger than that observed in stoichiometric single-crystal oxides.[12,15] As thicker films are grown, through multiple Fe evaporation/oxidation steps, for example, we observe that the valence-band structures quickly approach those observed in bulk oxides. With the growth of thicker films, one expects

that the spin polarization of the bulk material can be achieved.

In summary, we have grown thin Fe_3O_4 films on Cu(001) with excellent epitaxy. The films are well ordered and grow in highly oriented crystallites with micron dimensions. A model for the structure of the oxide and its epitaxy on Cu(001) has been presented, consistent with LEED and STM observations. These results suggest that thin films of Fe_3O_4 may be a useful candidate as a spin-polarized source or contact material in spin-sensitive transport devices.

This work was supported, in part, by the Louisiana State Board of Regents, the Center for Advanced Microstructures and Devices, and the National Science Foundation under Grant No. DMR-9802278.

[1] G. A. Prinz, Science **282**, 1660 (1998).
[2] R. J. Soulen *et al.*, Science **282**, 85 (1998).
[3] Z. Zhang and S. Satpathy, Phys. Rev. B **44**, 13 319 (1991).
[4] S. F. Alvarado, W. Eib, F. Meier, D. T. Pierce, K. Sattler, H. C. Siegmann, and J. P. Remeika, Phys. Rev. Lett. **34**, 319 (1975).
[5] J. F. Anderson, M. Kuhn, U. Diebold, K. Shaw, P. Stoyanov, and D. Lind, Phys. Rev. B **56**, 9902 (1997).
[6] J. A. Borchers, R. W. Erwin, S. D. Berry, D. M. Lind, E. Lochner, and K. A. Shaw, Appl. Phys. Lett. **64**, 381 (1994).
[7] Y. Q. Cai, M. Ritter, W. Weiss, and A. M. Bradshaw, Phys. Rev. B **58**, 5043 (1998).
[8] A. Barbieri, W. Weiss, M. A. Van Hove, and G. A. Somorjai, Surf. Sci. **302**, 259 (1994).
[9] M. W. J. Chase, in *NIST Chemistry WebBook, NIST Standard Reference Database Number 69* (http://webbook.nist.gov), edited by W. G. Mallard and P. J. Linstrom (National Institute of Standards and Technology, Gaithersburg, MD, 1998).
[10] D. Lind, S. D. Berry, G. Chern, and H. Mathias, Phys. Rev. B **45**, 1838 (1992).
[11] V. S. Smentkowski and J. T. Yates, Surf. Sci. **232**, 113 (1990).
[12] A. Koveshnikov, R. Madjoe, R. L. Stockbauer, and R. L. Kurtz, Surf. Sci. **442**, 223 (1999).
[13] J. Giergiel, J. Shen, J. Woltersdorf, A. Kirilyuk, and J. Kirschner, Phys. Rev. B **52**, 8528 (1995).
[14] D. T. Margulies, F. T. Parker, M. L. Rudee, F. E. Spada, J. N. Chapman, P. R. Aitchison, and A. E. Berkowitz, Phys. Rev. Lett. **79**, 5162 (1997).
[15] R. J. Lad and V. E. Henrich, J. Vac. Sci. Technol. A **7**, 1893 (1989).